Article:
Hawke, LGD, Huang, Q, Hassager, HO et al. (1 more author) (2015) Modifying the pom-pom model for extensional viscosity overshoots. Journal of Rheology, 59. 995. ISSN 0148-6055

https://doi.org/10.1122/1.4922060

Modifying the pom-pom model for extensional viscosity overshoots

L. G. D. Hawke[a)]

Department of Applied Mathematics, University of Leeds, Woodhouse Lane, Leeds LS2 9JT, United Kingdom

Q. Huang and O. Hassager

Department of Chemical and Biochemical Engineering, Technical University of Denmark, Lyngby DK-2800 Kgs., Denmark

D. J. Read

Department of Applied Mathematics, University of Leeds, Woodhouse Lane, Leeds LS2 9JT, United Kingdom

(Received 28 October 2014; final revision received 22 May 2015; published 11 June 2015)

Abstract

We have developed a variant of the pom-pom model that qualitatively describes two surprising features recently observed in filament stretching rheometer experiments of uniaxial extensional flow of industrial branched polymer resins: (i) Overshoots of the transient stress during steady flow and (ii) strongly accelerated stress relaxation upon cessation of the flow beyond the overshoot. Within the context of our model, these overshoots originate from entanglement stripping (ES) during the processes of normal chain retraction and branch point withdrawal. We demonstrate that, for a single mode, the predictions of our overshoot model are qualitatively consistent with experimental data. To provide a quantitative fit, we represent an industrial melt by a superposition of several individual modes. We show that a minimal version of our model, in which ES due to normal chain retraction is omitted, can provide a reasonable, but not perfect, fit to the data. With regard the stress relaxation after (kinematically) steady flow, we demonstrate that the differential version of tube orientation dynamics in the original pom-pom model performs anomalously. We discuss the reasons for this and suggest a suitable alternative. © *2015 The Society of Rheology*. [http://dx.doi.org/10.1122/1.4922060]

I. INTRODUCTION

The understanding of the flow properties of industrial melts, which have varied random long chain branching (LCB), is a significant step toward synthesizing polymers by design [McLeish (2002)]. Typically, in the nonlinear rheological regime and during startup of the flow, such polymer melts manifest severe extensional hardening even at

[a)]Author to whom correspondence should be addressed; electronic mail: laurence.hawke@uclouvain.be. Present address: Bio-and Soft Matter, Institute of Condensed Matter and Nanosciences, Université Catholique de Louvain, Croix du Sud 1, Louvain-la-Neuve B-1348, Belgium.

relatively slow flow rates. They also exhibit shear thinning as melts of linear polymers. These features are qualitatively captured by the pom-pom model of McLeish and Larson (1998). For a quantitative comparison with experimental data, the LCB structure is typically approximated by a superposition of independent (pom-pom) modes. In particular, Inkson *et al.* (1999) have demonstrated that a multimode version of the pom-pom model is able to account quantitatively for low-density polyethylene (LDPE) rheology in three different geometries of flows.

Despite the success of the multimode pom-pom (mPP) model of Inkson *et al.*, there is ambiguity about the extensional viscosity, $\eta_E(\dot{\epsilon})$, i.e., the steady state of the tensile stress growth coefficient (or transient uniaxial viscosity), $\eta_E^+(t, \dot{\epsilon})$. Specifically, in Münstedt-type [Münstedt and Auhl (2005)] and Meissner-type [Meissner and Hostettler (1994)] rheometers, the samples break or become inhomogeneous after a particular time (Hencky strain) in the hardening regime thus the steady state is not achieved [McKinley and Sridhar (2002)]. The same applies to SER rheometers [Sentmanat *et al.* (2005); Lentzakis *et al.* (2013); Hoyle *et al.* (2013)]. On the other hand, the filament stretching rheometer (FSR) is able to establish an effective steady state indicating that, for industrial melts like the so-called DOW 150 R sample, $\eta_E^+(t, \dot{\epsilon})$ undergoes an overshoot under kinematically steady flow [Rasmussen *et al.* (2005); Hoyle *et al.* (2013); Huang (2013)]. The observation of these overshoots is also supported by extensional viscosity measurements in a cross-slot flow [Hoyle (2011); Auhl *et al.* (2011); Hoyle *et al.* (2013)]. Nevertheless, some studies suggest that these overshoots are not a real material property but they emerge due to non-uniformities of the sample at high Hencky strains [Burghelea *et al.* (2011)].

Overshoots in engineering stress, under continuous extension, have been reported by Wang *et al.* (2011) for monodisperse and bidisperse polymer melts. However, such overshoots and real stress overshoots, measured by the FSR, are not the same since the two stresses (engineering and real) are defined differently. In particular, the real stress is the engineering one times $\exp(\dot{\epsilon}t)$, a geometric factor arising from the exponentially shrinking cross sectional area, and therefore, typically the real stress still increases while the engineering stress overshoots. Wang *et al.* have interpreted their measurements in terms of yielding through disintegration of the chain entanglement network and rubberlike rupture via non-Gaussian chain stretching leading to scission.

Using the FSR rheometer, it is also possible to measure the relaxation of stress following cessation of the extensional flow [Nielsen *et al.* (2008)]. Such measurements for LDPE melts [Huang *et al.* (2012)] imply that the stress relaxes faster when the flow is ceased after the overshoot (**AO** case) than before the overshoot (**BO** case).

These two observations of a stress overshoot, together with different stress relaxation behavior before and after the overshoot, are not predicted by the pom-pom model in either single or multimode (mPP) form. Recently, Hoyle *et al.* (2013) have introduced a variant of the original mPP theory, which successfully describes the extensional data of the DOW 150 R sample under steady flow. Specifically, they introduced an additional relaxation mechanism, driven from advection by the flow, into the dynamic stretch equation of the original theory. Nevertheless, their model is not tested against the stress relaxation data. In this context, we note that the extra relaxation term in Hoyle *et al.* is proportional to flow rate. Thus, upon cessation of flow, it is switched off and their model behaves as the original pom-pom model. Therefore, it would seem impossible for their model to predict the different stress relaxation behavior before and after the overshoot, even qualitatively.

Provided that branch point withdrawal is incorporated, another approach that enables overshoots in $\eta_E^+(t, \dot{\epsilon})$ is the so-called molecular stress function (MSF) model [Wagner and Rolón-Garrido (2008)]. This model has been tested against the data of Nielsen *et al.* (2006) on a melt of pom-pom shaped molecules. Primitive chain slip-link simulations also provide a

reasonable fit to these FSR data [Masubuchi *et al.* (2014)]. However, neither the MSF model nor the aforementioned slip-link simulations are tested against the stress relaxation data.

In the present paper, we propose a modification of the pom-pom model which includes both stress overshoots, and enhanced stress relaxation following the overshoot. We consider that to capture both of these observations requires an internal state variable within the model, which changes value during the stress overshoot. A candidate molecular-level explanation for such a change is "entanglement stripping (ES)": A reduction in the overall number of entanglements due to relative motion between entangled polymer strands. At the outset, it is worth defining precisely two related, hypothesized processes for disruption of entanglement structure in strong polymer flow, and to draw distinctions between them. One such process is commonly known as convective constraint release (CCR). In perhaps the most successful theoretical description of this process [Graham *et al.* (2003)], entanglement constraints are removed by flow, but *continually replaced* so that the effective tube constraint remains approximately constant, but the tube path takes local hops in proportion to shear rate, relaxing the tube orientation. In contrast, during the ES process considered here, the removed entanglements are *not* continually replaced, hence the tube diameter increases. It is important to distinguish these two separate processes, and (for the purposes of the present work) we shall consistently refer to the former as CCR and the latter as ES.

ES is frequently observed in slip-link models of entangled polymers under nonlinear flow [Masubuchi *et al.* (2012, 2014); Andreev *et al.* (2013)] and (since we performed this present work) has very recently been discussed in the context of linear polymers [Ianniruberto and Marrucci (2014); Ianniruberto (2015)]. There are also indications of ES in recent computer simulation, e.g., the work of Sefiddashti *et al.* (2015). However, in the context of branched polymers and the pom-pom model, the effects of ES are potentially very strong: (i) The onset of branch-point withdrawal within the model provides an occasion for a sudden and rapid increase in the amount of ES. Furthermore, (ii) we expect that ES would give rise to significantly altered relaxation rates, since relaxation times in branched polymers are exponentially dependent on the degree of entanglement. The purpose of the present work is to explore effects (i) and (ii) above within the semiphenomenological framework of the pom-pom model. We shall demonstrate that, at a qualitative level, reasonable modifications to the pom-pom model in line with the ES hypothesis can qualitatively capture the observed experimental phenomena in startup extension and stress relaxation. To quantitatively compare our model with the FSR data, we decompose the LCB structure into a collection of individual pom-pom modes in line with the approach of Inkson *et al.* (1999). We consider that our successful comparison with experimental data is indicative that ES is a viable hypothesis to explain the stress overshoots and anomalous stress relaxation. However, the mPP approach necessarily involves a large number of fitting parameters; thus, confirmation of this proposed mechanism requires a more detailed molecular-level investigation.

II. EXPERIMENTAL DETAILS

The measured material is a highly branched LDPE DOW 150 R. The properties of the material are listed in Table I. The linear rheology has been reported by Hassell *et al.* (2008). The nonlinear rheology in extensional flow has been reported by Hoyle *et al.* (2013) using three different rheometers including the FSR [Bach *et al.* (2003)]. In Hoyle *et al.* (2013), the transient stress of DOW 150 R from the FSR was measured two to three times for each stretching rate, and the reported data are the denoised data after wavelet processing [Huang *et al.* (2012)]. This processing splits the raw data set into two parts, approximation and details (noise), and the former part is then selected to represent the result. It is possible to

TABLE I. Material properties of the LDPE resin DOW 150 R.

M_w(kg/mol)	M_w/M_n	T(°C)	η_0(kPa · s)
242	11	160	368

retrieve the raw data set by adding the noise part to the approximation part; details of wavelet processing and an example of comparison between the raw and the denoised data can be found in Huang *et al.* (2012). The experimental error was not reported in Hoyle *et al.* (2013). The upper panel of Fig. 1 shows the extensional (steady state) viscosity, $\eta_E(\dot{\epsilon})$, of DOW 150 R with an error bar based on the raw data from the FSR at 160 °C.

In the current paper, stress relaxation measurements for DOW 150 R have been performed using the same FSR. Prior to making a measurement, the material was hot pressed into cylindrical test specimens at 160 °C, with radius $R_0 = 4.5$ mm and length $L_0 = 2.5$ mm, giving an aspect ratio $\Lambda_0 = L_0/R_0 = 0.556$. During the measurements, the force $F(t)$ was measured by a load cell and the diameter $2R(t)$ at the midfilament plane was measured by a laser micrometer. At small deformation in the startup of the extensional flow, part of the stress difference comes from the radial pressure variation due to the shear stress components in the deformation field. This effect may be compensated by

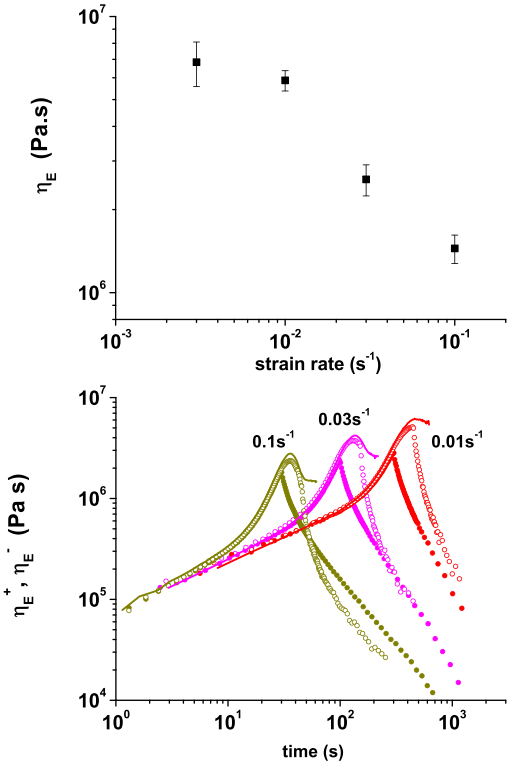

FIG. 1. Upper panel: Extensional (steady state) viscosity of DOW 150 R vs strain rate at 160 °C measured by the FSR. The error bars are the standard deviations of the transient raw data in the steady-state range. For the lowest rate, the force during extension is lower than the other rates, and the raw data is more scattered. Therefore, the standard deviation for the lowest rate is larger. Bottom: Transient extensional viscosity of DOW 150 R vs of time at 160 °C with $\dot{\epsilon} = 0.1, 0.03$, and $0.01\,s^{-1}$. For each rate, the flow was stopped at a Hencky strain of $\epsilon_0 = 3$ (filled symbols) and 4.5 (open symbols), respectively. The lines are the FSR measurements of uniaxial extension taken from Hoyle *et al.* (2013).

a correction factor as described by Rasmussen *et al.* (2010). The Hencky strain and the mean value of the stress difference over the midfilament plane are then calculated as

$$\epsilon(t) = -2\ln(R(t)/R_0), \tag{1}$$

$$\langle \sigma_{zz} - \sigma_{rr} \rangle = \frac{F(t) - m_f g/2}{\pi R(t)^2} \cdot \frac{1}{1 + \left(R(t)/R_0\right)^{10/3} \cdot \exp\left(-\Lambda_0^3\right) \Big/ \left(3\Lambda_0^2\right)}, \tag{2}$$

where m_f is the weight of the filament and g is the gravitational acceleration. The strain rate is defined as $\dot{\epsilon} = d\epsilon/dt$.

The measurements were performed at three different constant strain rates in the startup phase. A recently updated control scheme [Marin *et al.* (2013)] is employed in the FSR to ensure accurate constant strain rate. Note that the overshoots have been observed both before and after the update of the control scheme, and their magnitude is the same. The tensile stress growth coefficient in the startup of the flow is defined as $\eta_E^+ = \langle \sigma_{zz} - \sigma_{rr} \rangle / \dot{\epsilon}_0$. For each rate, the flow was stopped at a Hencky strain $\epsilon_0 = 3$ and $\epsilon_0 = 4.5$, respectively. The midfilament radius in the stress relaxation phase was kept constant by the active control scheme, giving $\dot{\epsilon} = 0$. The tensile stress decay coefficient is defined as $\eta_E^- = \langle \sigma_{zz} - \sigma_{rr} \rangle / \dot{\epsilon}_0$, where $\dot{\epsilon}_0$ is the strain rate in the startup of the flow.

The bottom panel of Fig. 1 shows the results of the stress relaxation measurements for DOW 150 R at 160 °C. The presented data are the denoised data after wavelet processing [Huang *et al.* (2012)]. With the strain rate $\dot{\epsilon}_0 = 0.1\,\mathrm{s}^{-1}$, the stress relaxation measurement at $\epsilon_0 = 4.5$ (after the overshoot—**AO** case) shows a remarkably faster decrease in the tensile stress decay coefficient compared with the measurement at $\epsilon_0 = 3$ (before the overshoot—**BO** case), which is in agreement with the observations by Huang *et al.* (2012) for another two LDPE melts. At this rate, strong crossing between the **AO** and **BO** curves ensues. With decreasing strain rate, though stress relaxation remains faster after the overshoot than before the overshoot, there appears to be less tendency toward crossing. Nevertheless, the data at the two lowest measured rates are cut short, due to the force being too small to obtain reliable measurements; therefore, crossing behavior cannot be ruled out completely; possibly if data were taken for longer times, or relaxation after different applied strains, it might be possible to find crossing behavior even for lower rates.

III. MODELING THE RHEOLOGY OF LDPE

A. The pom-pom model

In this section, we briefly review the pom-pom model. A pom-pom molecule consists of two q-armed stars that are connected by a linear backbone. It relaxes its configuration hierarchically from outward (arms) to inward (backbone). However, the process of arm retraction is considered instantaneous on the flow timescale (that is, on average, the arms are considered unstretched and isotropically oriented), and therefore, it is the backbone that contributes to the polymer stress. There are two dynamic variables: The preaveraged backbone orientation, $\mathbf{S}$ and the preaveraged backbone stretch, λ. Two options were given for the evolution equation of $\mathbf{S}$ [McLeish and Larson (1998)]: An integral form, based on the Doi–Edwards model, and an approximate differential form which was

$$\mathbf{S} = \frac{\mathbf{A}}{\mathrm{tr}\mathbf{A}}, \text{ with } \frac{d\mathbf{A}}{dt} = \mathbf{K}\cdot\mathbf{A} + \mathbf{A}\cdot\mathbf{K}^{\mathrm{T}} - \frac{1}{\tau_d}\left(\mathbf{A} - \frac{1}{3}\mathbf{I}\right), \tag{3}$$

where **K** is the velocity gradient tensor, **A** is an auxiliary tensor, and τ_d is the orientation relaxation time. Both the differential and integral forms of the pom-pom orientation equation are based on the mathematical description of deformation of line-segments (the tube path) in a flow-field, with relaxation due to tube escape. Each form makes different mathematical approximations to achieve a closed equation, and both neglect physical processes such as constraint release. At the level of a single pom-pom mode, mathematical differences between the two forms can be teased out, and one may spend time questioning which is the more "correct" description of orientation. However, the practical utility of the pom-pom model is in its multimode incarnation, as a tool to describe rheology of broadly polydisperse branched polymer resins. In this application, most differences between the integral and differential forms of the orientation equation are masked by the presence of many modes. The principle advantage of the differential form, and the reason for its widespread use, was in its utility in complex flow calculations. However, we shall discuss below a limitation of the differential form of the model, specifically with respect to stress relaxation after strong extensional flow, and propose an alternative differential orientation equation.

The evolution equation for λ is as follows:

$$\frac{d\lambda}{dt} = \lambda \mathbf{K} : \mathbf{S} - \frac{1}{\tau_s}(\lambda - 1), \tag{4}$$

where τ_s is the stretch relaxation time. Equation (4) holds while $\lambda < q$. When $\lambda = q$, the stretch achieves the so-called maximum stretch condition. Then, branch point withdrawal occurs, i.e., the branch points are withdrawn into the backbone tube to maintain the maximum stretch (see also Fig. 2 below).

In its multimode version, the model contains four parameters per mode, namely, G_0 (the plateau modulus), τ_d, τ_s, and q. The first two parameters control the linear viscoelastic properties of the melt. They are obtained by fitting G' and G'' to a finite spectrum of Maxwell modes. The last two parameters determine the nonlinear response of the melt, and thus, they are typically obtained by matching data from transient shear or extensional flow.

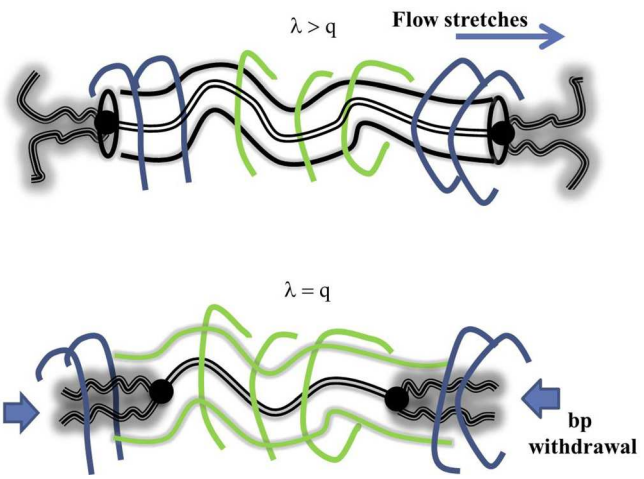

FIG. 2. Up: A given backbone, prior to branch point withdrawal, entangled with surrounding chains (backbones). The flow tends to stretch the backbone beyond the maximum stretch hence $\lambda > q$. Bottom: Branch point withdrawal occurs since the maximum stretch, $\lambda = q$, should be maintained. This process is instantaneous on the flow timescale and hence some entanglements are stripped off. Here, the backbone entangles with fewer chains, and therefore, it is confined within a dilated tube.

Here, it should be clarified that the present model (as was the case with the original pom-pom model) is developed with a view to describe the flow properties of randomly branched, polydisperse industrial melts rather than specific model branched polymers. While the rheology of "model" polymer melts can often be described using the pom-pom model, a frequent problem is that fitting parameters do not always correspond to the known molecular structure. For example, when a single mode version of these models (using $q = 3$) is compared against data for a pom-pom melt [Nielsen *et al.* (2006)], the level of strain hardening is highly underestimated (possibly because some of the flow rates in that experiment exceeded the inverse Rouse time of the molecules).

B. The overshoot model: The physical concept

Central to the modification of the original model is the assumption that, under fast flows and during the process of chain retraction, some of the backbone-backbone entanglements can be stripped off. In this context, the point where a pom-pom backbone achieves its maximum stretch represents a sudden increase in the rate of chain retraction and, in turn, in the degree of ES and so can be responsible for a sudden loss of entanglements; this idea is illustrated schematically in Fig. 2.

To describe quantitatively the effect of ES, we introduce the dynamic variable Ψ, which represents the fraction of surviving entanglements at a particular time. We also introduce Ψ_w, a parameter that denotes the minimum fraction of surviving entanglements; in the absence of ES $\Psi_w = \Psi = 1$.

From the conceptual point of view, the qualitative consequences of ES are as follows: As ES goes on, the backbone tube gradually dilates and as a result the relaxation times (τ_d and τ_s) speed up. Hence, in our model, these relaxation times have a dependence on Ψ; therefore, they are time dependent [see Eq. (8) below].

C. The overshoot model: The constitutive equation

The equation for the stress reads

$$\boldsymbol{\sigma} = 3G_0\,\Psi\,\lambda^2\,\mathbf{S}, \tag{5}$$

instead of $\boldsymbol{\sigma} = 3G_0\ \lambda^2\,\mathbf{S}$ (for a single mode) of the mPP model [Inkson *et al.* (1999)]. The extra factor of Ψ accounts for the effective dilution of the entanglement network due to ES. From Eq. (5), it is apparent that decreases in Ψ naturally lead to overshoots. As regards the multimode version, the stress contribution of all the (N) modes is additive; that is, the total stress is given by

$$\boldsymbol{\sigma} = \sum_{i=1}^{N} \boldsymbol{\sigma}_i = 3\sum_{i=1}^{N} G_{0_i}\,\Psi_i\,\lambda_i^2\,\mathbf{S}_i. \tag{6}$$

In the following, we restrict our description to the experiments performed in the FSR rheometer, as opposed to a general deformation history. Here, an initial flow of constant extension rate is applied. During the extensional flow, ES may occur, and the backbone tube gets wider. Following this, the flow may be stopped, and the melt relaxes. During the relaxation phase, chain retraction and ES eventually stops, so that entanglements begin to be replaced and the tube gets thinner again. In the following, we first consider writing the constitutive equation, in terms of backbone orientation, $\mathbf{S}$, and stretch, λ, during the initial extensional flow, with ES taking place. We then examine the modifications that must be made as entanglements are reformed during the relaxation phase. The process that gives rise to entanglement reformation is tube renewal (reptation of the

backbones); in other words, we assume that the chains will eventually re-entangle with surrounding chains as they relax their orientation.

We note that **S** is the orientation tensor $\langle \mathbf{uu} \rangle$ of a tube segment at the current degree of ES: That is, **u** is directed along the tube path defined by the surviving backbone-backbone entanglements only. As an example, consider the two tubes shown in Fig. 3; a thin one at a low degree of ES, and a fatter one representing the tube that will apply when some more of the entanglements are stripped away. At equilibrium, the orientation vectors **u** of both tubes are isotropically distributed. In the figure, we depict two tube segments (a thin one and a fat one) which just happen to have the same orientation **u**. During the initial startup flow, provided all the entanglements remain in place, these two tube vectors will undergo exactly the same strain history, i.e., their orientation vectors after deformation will be identical to one another. Similarly, if the chain escapes the thin tube (thus allowing reorientation) then the chain also escapes the fat tube (allowing it to reorient in the same way). So, we conclude that, before any ES occurs, the orientation tensor of the fat and thin tubes are identical. When the ES does actually occur (and the thin tube disappears) the perhaps surprising conclusion is that the orientation tensor of the new, fatter, tube is identical to the orientation tensor for the original thinner tube. So, during the initial flow and ES phase, the evolution equation for the orientation tensor remains unchanged, unaffected by the degree of ES. Similarly, since the fractional amount of chain retraction is also the same for both fat and thin tubes, the stretch equation is also unchanged during the startup flow.

This situation does not remain when the flow is stopped and entanglements are replaced. In this case, the newly formed thinner tube will take a configuration which is (locally) at equilibrium inside the fatter tube (i.e., the thin and fat tubes no longer have identical strain and relaxation history). We shall deal with this situation below, using the criterion that replacing entanglements should not increase the deviatoric stress. We will find that we need to add extra terms to the orientation and stretch equations. For more general strain histories than considered here, with repeated phases of ES and reformation, it would be necessary to include a more complete representation of the nested tube structure at different dilutions, for example, using the formalism in Read *et al*. (2012).

For the evolution equation of the backbone stretch, we retain the differential equation of the original model, i.e., Eq. (4). For the time evolution of the backbone orientation, we pursue solely a differential formulation (recall that the original pom-pom model was presented in both integral and differential form). There are two reasons for our choice, (i) ease of use in flow computation, and (ii) in the case of entanglement reformation dealt with below, the mathematics is more naturally expressed in differential form. Hence, for the backbone orientation, we use the following differential equation:

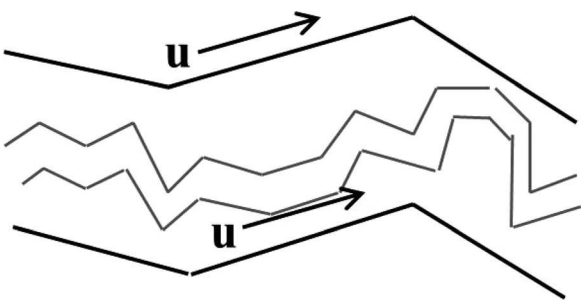

FIG. 3. Thin tube: The backbone tube at the current degree of ES. Fat tube: The backbone tube that will apply when some more of the entanglements are stripped away. Here, we depict two tube segments (a thin one and a fat one) which just happen to have the same orientation **u**. For more details see the text.

$$\frac{d\mathbf{S}}{dt} = \mathbf{K}\cdot\mathbf{S} + \mathbf{S}\cdot\mathbf{K}^{\mathrm{T}} - 2\mathbf{S}(\mathbf{K}:\mathbf{S}) - \frac{1}{\mathcal{B}\tau_d}\left(\mathbf{S} - \frac{\mathbf{I}}{3}\right), \tag{7}$$

where we test three different versions of this equation in which $\mathcal{B}$ takes the values tr $\mathbf{A}$, λ^2, or 1. The reason for exploring these three versions will become apparent when we examine the shear response, and the relaxation behavior following a step strain, below.

The first version of Eq. (7), in which $\mathcal{B} = \mathrm{tr}\mathbf{A}$, exactly corresponds to the original pom-pom model, i.e., to Eq. (3) when it is re-expressed in terms of $\mathbf{S}$ rather than in terms of $\mathbf{A}$. In the second version, the chain is considered to diffuse within a stretched backbone tube hence the orientation relaxation time is amplified by $\mathcal{B} = \lambda^2$ [Verbeeten *et al.* (2001); Clemeur *et al.* (2003, 2004)]. This form of the orientation equation can also be derived from the stretching version of the Rolie-Poly model for linear polymers [Graham and Likhtman (2003)] in the absence of constraint release, by splitting the stress tensor in that model into tensor orientation and scalar stretch components. The third version corresponds to $\mathcal{B} = 1$. It is obvious that the rate of tube reconfiguration in the three different versions of Eq. (7) is $(\mathrm{tr}\mathbf{A}\tau_d)^{-1}$, $(\lambda^2\tau_d)^{-1}$, and τ_d^{-1}, respectively.

The relaxation times in Eqs. (4) and (7) are not time independent, but they are modified as follows:

$$\tau_d = \tau_{d_0}\exp\left(h(\Psi - 1)\right)\exp\left(-\nu(\lambda - 1)\right), \tag{8a}$$

$$\tau_s = \tau_{s_0}\exp\left(h(\Psi - 1)\right)\exp\left(-\nu(\lambda - 1)\right), \tag{8b}$$

where τ_{d_0} and τ_{s_0} are, respectively, the orientation and the stretch relaxation time in the absence of ES and drag-strain coupling (hereafter, referred to as the bare relaxation times). The factor $\exp\left(-\nu(\lambda - 1)\right)$, where $\nu = 2/(q-1)$, is due to the drag-strain coupling effect introduced by Blackwell *et al.* (2000). The other exponential term reflects the speed up of the relaxation times due to ES [see Eq. (10) below]. This term is derived as follows. In branched polymers, the relaxation times are exponentially dependent on the arm entanglement length (or number of arm entanglements), Z_a, as follows:

$$\tau_d, \tau_s \propto \exp\left(\nu' Z_a\right) = \exp\left(\nu'(Z_{a,0} - Z_s)\right), \tag{9}$$

where ν' is a numerical constant of order unity, $Z_{a,0}$ is the number of arm entanglements in the limit of no ES, and $Z_s (= Z_{a,0} - Z_a)$ is the number of stripped entanglements (which is a time dependent quantity). The $\exp\left(h(\Psi - 1)\right)$ term in Eq. (8) reflects the $\exp\left(-\nu' Z_s\right)$ term in Eq. (9); h is a parameter that accounts for the proportionality of τ_d and τ_s on the timescale for a complete arm retraction and, in turn, on Z_a. The factor of Ψ arises from the dilution of the entanglement network as follows:

$$\begin{aligned}\exp(-\nu' Z_s) &= \exp\left(-\nu'(Z_{a,0} - Z_a)\right),\\ &= \exp\left(-\nu'\frac{M_a}{M_{e,0}}(1 - \Psi)\right),\\ &= \exp(h(\Psi - 1)),\end{aligned} \tag{10}$$

where M_a is the arm molecular weight and $M_{e,0}$ is the entanglement molecular weight in the limit of no ES. From Eq. (10), it is clear that increases in h lead to a more rapid decrease in relaxation times relative to their equilibrium value. Note that the term arm entanglement length (or arm molecular weight) refers to the entanglement length of the branching layers (of the LCB structure) that are adjacent to the branch that the pom-pom

backbone is supposed to represent. We are actually assuming, for the sake of simplicity, that the degree of ES is the same at a given branching layer and its adjoining branches. In practice, the degree of ES will be similar, but not exactly the same. To represent the physics more accurately, i.e., to account for the fact that entanglements are communal in determining relaxation times, one might couple the relaxation time of one mode to the degree of ES of other pom-pom modes (which would then represent the adjoining branches). Indeed, in the course of developing this work, we did attempt schemes in which the modes were coupled together. Nevertheless, this coupling introduced yet more (arbitrary) parameters in the model and was thus not very satisfactory from that point of view. A full treatment of the aforementioned physics would require a detailed tube model, in which tube dynamics equations are solved over the many randomly branched structures appropriate for LDPE. Such a huge task has never been successfully implemented to our knowledge and is certainly beyond the scope of this paper. Finally, we note that Eqs. (8)–(10) are retained during entanglement reformation.

We now consider the dynamics of orientation and stretch during entanglement reformation, which occurs (typically) after the flow is stopped. Here, as entanglements are reformed, the chain becomes localized by a thinner tube which locally equilibrates within a fatter tube. In this case, one should include an extra "correction" term in Eqs. (4) and (7), such that reformation of entanglements does not increase the deviatoric components of the stress. These correction terms are obtained as follows. Consider the equilibration process of tube 1 (thin tube) within tube 2 (fat tube). According to the work of Auhl *et al.* (2009) for a thin tube equilibrated inside a fat tube, the orientation and stretch of the thin tube and the fat tube are related through

$$\lambda_1^2 \mathbf{S}_1 = \frac{1}{n}\lambda_2^2 \mathbf{S}_2 + \frac{1}{3}\left(1 - \frac{1}{n}\right)\mathbf{I}, \tag{11}$$

where $\mathbf{I}$ is the unit tensor and n is the number of thin tube segments within each fat tube segment. Here, n can be approximated by the ratio of the ES factors for the two tubes, i.e., by Ψ_1/Ψ_2, and therefore, the previous equation is re-expressed as

$$\lambda_1^2 \mathbf{S}_1 = \frac{\Psi_2}{\Psi_1}\lambda_2^2 \mathbf{S}_2 + \frac{1}{3}\left(1 - \frac{\Psi_2}{\Psi_1}\right)\mathbf{I}. \tag{12}$$

By taking the two tube diameters almost identical, assuming only a small change in Ψ, and noting that the trace of $\mathbf{S}$ remains constant, it can be shown that the effective changes in λ and $\mathbf{S}$ due to a small change in Ψ arising from Eq. (12) are

$$\left(\frac{d\lambda}{dt}\right)_+ = \left(\frac{1-\lambda^2}{2\lambda\Psi}\right)\frac{d\Psi}{dt}, \tag{13a}$$

$$\left(\frac{d\mathbf{S}}{dt}\right)_+ = \left(\frac{\Psi\mathbf{I} - 3\Psi\mathbf{S}}{3\lambda^2\Psi^2}\right)\frac{d\Psi}{dt}. \tag{13b}$$

Hence, when $d\Psi/dt > 0$, Eqs. (13a) and (13b) should be added to the right-hand side of Eqs. (4) and (7), respectively. In practice, one can ignore these extra terms in the *normal case* (NC) (cf. Table IV of Appendix B), as $d\Psi/dt$ becomes positive during the relaxation phase only. With these extra terms, the deviatoric components of the stress are unaltered by entanglement reformation.

We now move on to derive an expression for the time evolution of Ψ, the fraction of surviving entanglements. Ψ is determined by two opposing factors: On the one hand,

chain retraction causes ES either before or after the maximum stretch [first term of Eq. (14)], on the other hand, melt re-equilibration tends to keep the fraction of surviving entanglements to its equilibrium value of unity [second term of Eq. (14)]. We assume that melt re-equilibration occurs on the timescale of orientation relaxation. Therefore, we express the time evolution of Ψ as follows:

$$\frac{d\Psi}{dt} = w(\Psi - \Psi_w) - \frac{1}{\mathcal{B}\tau_d}(\Psi - 1), \tag{14}$$

where $\mathcal{B} = \text{tr}\mathbf{A}$, λ^2 or 1 as in Eq. (7). Ψ_w is the minimum fraction of surviving entanglements. The physical meaning of this parameter is described as follows. In any flow situation, entanglements are removed via the "stripping" process described herein. At the same time, entanglements may be replaced as convection of chains brings them closer together (this allows entanglements to be formed as two chains "meet" each other in the middle of the chains as they are brought together by the flow). In some early treatments of CCR, it was thought that the ES process was exactly balanced by this entanglement reformation process, such that the tube diameter remained constant. If the two processes do not exactly balance, the number of entanglements will reduce, but not necessarily to zero because entanglements can be created by flow. In our view, this is the physical reason allowing the use of an impassable lower bound for the fraction of surviving entanglements.

The retraction rate, w, is defined as the difference between the actual rate of stretching and the rate of stretching due to flow alone

$$w = \frac{1}{\lambda}\left(\frac{d\lambda}{dt} - \lambda(\mathbf{K} : \mathbf{S})\right). \tag{15}$$

We stress that, for the flow conditions examined in this work, w is always negative. By substituting Eq. (4) into Eq. (15), one arrives at

$$w = \begin{cases} -(\lambda - 1)/(\tau_s\lambda) & \text{for } \lambda < q \\ -\mathbf{K} : \mathbf{S} & \text{for } \lambda \geq q. \end{cases} \tag{16}$$

Similar equations have been used by Ianniruberto and Marrucci (2014) and Ianniruberto (2015) in the context of linear polymers.

Compared to the mPP model that has four parameters per mode, we have introduced two additional parameters per mode, namely, Ψ_w and h, the minimum fraction of surviving entanglements, and the number of arm entanglements before the onset of ES, respectively. Moreover, in our model, there are three evolution differential equations per mode rather than two [see Eqs. (4), (7), and (14)]. Note that, for the moment, we will consider all versions of Eqs. (7) and (14); therefore, we will essentially consider three constitutive equations. Hereafter, the constitutive equations in which $\mathcal{B} = \text{tr}\mathbf{A}$, $\mathcal{B} = \lambda^2$, and $\mathcal{B} = 1$ will be referred to as CE-A, CE-B, and CE-C, respectively.

IV. SINGLE MODE PREDICTIONS

A. Testing the three versions of the evolution equation for the backbone orientation

In this section, we demonstrate that CE-B is the most suitable constitutive equation among the three versions of Eq. (7) for simultaneously fitting experimental data of

transient shear, and relaxation following uniaxial extension. We are able to draw this conclusion independently of any discussion of ES, which is omitted in the present section. The single mode under consideration is parameterized as follows: $\tau_{d_0}/\tau_{s_0} = 2$, $q = 12$, $\Psi_w = 1$, and $h = 0$; the values of the linear parameters, G_0 and τ_{d_0}, correspond to the slowest mode (8th) of the pom-pom spectra of Tables II and III below (cf. Appendix A). The choice $\Psi_w = 1$ ensures that ES is quenched in the model.

Figure 4 shows comparisons of the three different constitutive equations at two different flows, i.e., relaxation following extensional flow (left) and shear (right). Upper panels show the transient viscosity vs time while the bottom panels show the corresponding orientation dynamics (that is, $S_{xx} - S_{yy}$ and S_{xy} for relaxation and shear, respectively.) From Fig. 4, the following two conclusions may be drawn.

First, constitutive equation A, which corresponds to the original pom-pom equation (when $\Psi_w = 1$), is very poorly behaved in relaxation after extensional flow and must be rejected; here, $S_{xx} - S_{yy}$ starts to decrease almost two decades after the cessation of the flow due to the unnaturally low rate of tube reconfiguration, which is determined by the $(\mathrm{tr}\mathbf{A}\tau_d)^{-1}$ term. In this context, we note that the quantity tr**A** carries *no physical meaning* and, moreover, is unbounded for high strain rates. It was originally introduced, within the differential version of the pom-pom model, as an approximate means to obtain the tube orientation, **S**. So, it is unreasonable that it should produce such a strong effect on the constitutive response. On the other hand, CE-B and CE-C are more realistic than CE-A; in both cases, the relaxation of the orientation is governed by physical parameters ($\tau_d\lambda^2$ or τ_d, respectively). For the present parameterization, in which the stretch and orientation

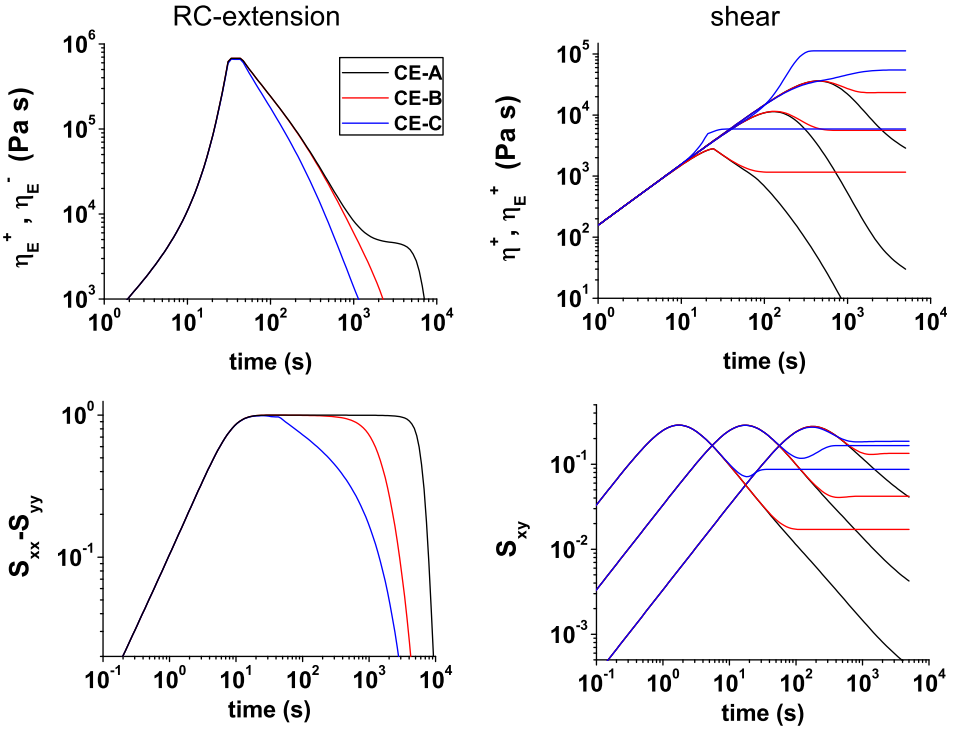

FIG. 4. Left: (upper) η_E^+, η_E^- vs time for all three constitutive equations at $\dot{\epsilon} = 0.1\mathrm{s}^{-1}$. The flow is ceased at $t \simeq 45\mathrm{s}$ ($\epsilon_0 = 4.5$). (Bottom) the corresponding orientation alignment. Right: (upper) η^+ vs time. (Bottom) the corresponding shear component of the orientation tensor. In all panels, the black, red, and blue lines refer to CE-A, CE-B, and CE-C, respectively. In all cases, ES is quenched.

relaxation times are comparable, CE-C relaxes significantly faster than CE-B. This feature makes the fitting of relaxation data more straightforward with CE-C than CE-B. However, we must reject CE-C on other grounds, as we shortly demonstrate. It should be mentioned here that for the chosen parameterization, the three constitutive equations engender the same stretch dynamics (not shown). Hence, the differences among them are solely attributed to the orientation dynamics, i.e., Eq. (7).

Second, constitutive equation C is very poorly behaved in shear flow and must be rejected as well. As it is readily seen from the right, upper panel of Fig. 4 with this equation shear hardening behavior is observed. This is, presumably, the practical reason why this form of differential orientation equation was rejected by McLeish and Larson (1998). They attributed the behavior to the fact that the S_{xy} element of the orientation tensor does not exhibit the right asymptotic form [McLeish and Larson (1998)]. In particular, S_{xy} manifests high steady state values which lead to high stretch through the $\mathbf{K} : \mathbf{S}$ coupling term in the stretch equation. Again, CE-B exhibits an intermediate behavior between those of CE-A and CE-C, and in particular, CE-B does not show the anomalous shear-hardening exhibited by CE-C. Therefore, in what follows, CE-B will be adopted.

We may note, here, that the integral form of the orientation equation used by McLeish and Larson (1998) is also a suitable candidate model within the terms of the present discussion: It is well behaved under shear flow, and its orientation relaxation time is not strongly perturbed in extensional flow, i.e., it does not suffer the same failing as the differential model CE-A proposed by McLeish and Larson (1998). The main reason for not adopting the integral model in our work is that Eqs. (11)–(13) for entanglement reformation are most naturally cast in differential form.

B. Constitutive equation B: Varying the values of the model parameters

Here, in contrast to Sec. IV A, we allow ES. We study how a reference mode (parameterized by $G_0 = 157$ Pa, $\tau_{d_0} = 848$ s, $\tau_{d_0}/\tau_{s_0} = 1.5$, $q = 12$, $\Psi_w = 0.5$, and $h = 1$) behaves with respect to variations in the values of the model parameters Ψ_w and h. Specifically, Figs. 5 and 6 refer to variations in Ψ_w and h, respectively. The left panels depict the NC, i.e., the flow condition in which the polymer melt is subjected to steady, uniaxial

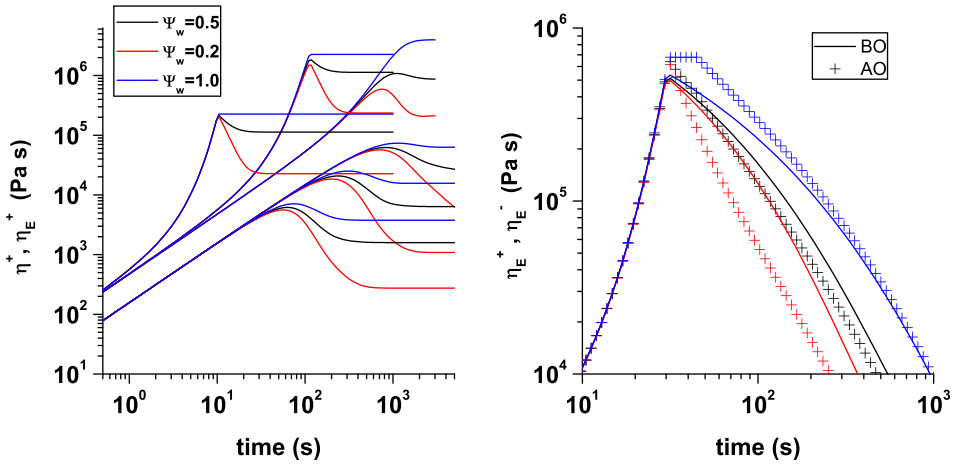

FIG. 5. Transient viscosity vs time for CE-B with varying Ψ_w (see labels). Left panel: NC for uniaxial extension and shear. Right panel: RC for extension. For the latter case, symbols refer to cessation of the flow after the overshoot (**AO**) while lines refer to cessation of the flow before the overshoot (**BO**).

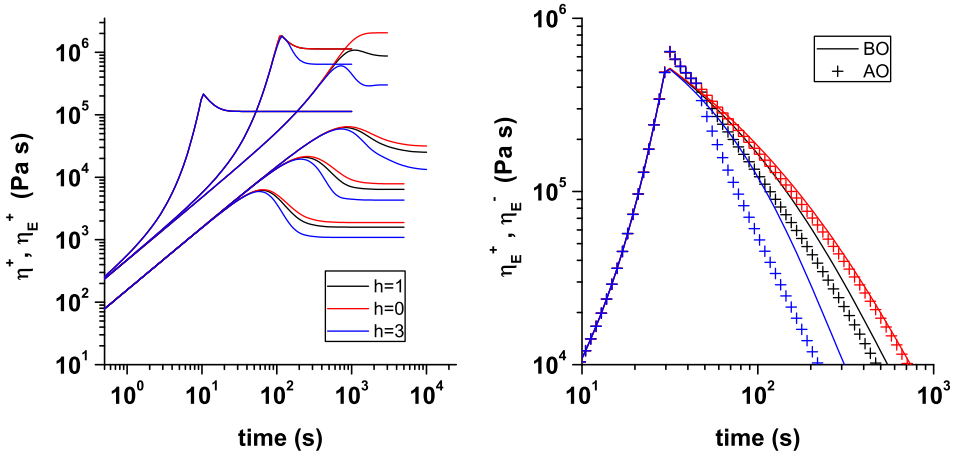

FIG. 6. Same as Fig. 5 with varying h (see labels).

extensional flow, or/and steady shear. Here, the strain rates are the following: $\dot{\epsilon} = 0.003\,\mathrm{s}^{-1}$, $\dot{\epsilon} = 0.03\,\mathrm{s}^{-1}$, and $\dot{\epsilon} = 0.3\,\mathrm{s}^{-1}$. Hereafter, these rates will be referred to as r2, r4, and r6, respectively. (For easy reference, the main abbreviations used in this paper are summarized in Table IV of Appendix B.) In the same figures, the right panels show the *relaxation case* (RC), i.e., the respective case that involves cessation of the extensional flow at a particular time. In this case, the strain rate is $\dot{\epsilon} = 0.1\,\mathrm{s}^{-1}$ (r5). Notice that, for the NC at extension, the maximum stretch condition is always reached at the three highest rates (r4, r5, and r6).

With respect to Fig. 5, we note that decreases in Ψ_w, the minimum fraction of surviving entanglements, correspond to higher ES. The left panel of this figure demonstrates that, by adjusting Ψ_w, one can readily control the magnitude of the overshoot and, in turn, the extensional viscosity (steady state) both in shear and extension; that is, decreases in Ψ_w lead to larger overshoots and hence to lower steady states. As regards the extensional flow, when the maximum stretch condition is achieved, the dominant contribution to the overshoot comes from ES. (There is also a small contribution from an overshoot in the orientation alignment.) Otherwise, there is an additional contribution from an overshoot in stretch. Also, from the upper panel of Fig. 5, it is obvious that, for $\Psi_w = 1$, the predictions of the present model are qualitatively similar to the predictions of the original model, i.e., after its maximum, $\eta_E^+(t, \dot{\epsilon})$ exhibits a plateau, since there is no ES.

Concerning the RC (left panel of Fig. 5) and, in particular, the **AO** case, we observe the following two features: First, in the time interval between the maximum of the transient viscosity and cessation of the flow, i.e., in the interval $31\,\mathrm{s} \lesssim t \lesssim 45\,\mathrm{s}$, the transient viscosity decays faster with decreasing Ψ_w since the level of ES increases. We may note, here, that the only time where stripping is still occurring is in this time interval, in which the transient viscosity manifests an initial sharp drop. Then, entanglements gradually start to reform. (Recall, however, that ES can also happen during the flow, i.e., in the NC.) For $\Psi_w = 1$, it remains constant in the aforementioned interval since ES is quenched in the model. Second, upon cessation of the flow, it continues to drop faster with decreasing Ψ_w. This is because lower values of Ψ_w and, in turn, lower values of Ψ lead to faster stretch and orientation relaxation times, and thus, they lead to a more rapid relaxation behavior. The latter feature is also seen in the **BO** case.

With respect to Fig. 6 and, in particular, the NC we note that generally the response to increases in h is similar to the response to decreases in Ψ_w. In other words, higher values of h lead to larger overshoots in both shear and extension. We now turn the discussion to the RC (right panel). For the **AO** case, in the time window between the maximum of the transient viscosity and flow cessation, the relaxation behavior is independent of h. This is due to the fact that Ψ_w is fixed hence ES is of similar strength for all considered values of h. Upon cessation of the flow, and for both cases (**AO** and **BO**), the tensile stress decay coefficient, $\eta_E^-(t,\dot{\epsilon})$, decays faster with increasing h since orientation and stretch relaxation speed up.

According to the right panels of Figs. 5 and 6, the overshoot model forecasts that the stress relaxes faster when the flow is ceased after the overshoot than before the overshoot. Provided that ES is switched on (i.e., $\Psi_w \neq 1$), this is a typical behavior of the model for slow modes, and it is qualitatively consistent with the FSR relaxation data. It is attributed to the significant ES caused by branch point withdrawal, which in turn results in much stronger drop in the relaxation times (τ_d and τ_s) when the flow is stopped after the overshoot than before the overshoot. On the other hand, when ES is switched off (i.e., $\Psi_w = 1$) the aforementioned behavior is not seen (see Fig. 5). This feature shows that the original pom-pom model is incapable of reproducing the relaxation behavior of the FSR measurements.

C. A rough guide for fitting data with the overshoot model

In this section, we briefly discuss the effects of the different parameters (τ_{d_0}/τ_{s_0}, q, Ψ_w, h) from the perspective of fitting transient viscosity data from an industrial melt. To fit such data, one needs a spectrum of modes. Therefore, one should bear in mind that at a given rate, $\dot{\epsilon}$, several modes may contribute to the stress, and the matching of the data could possibly require adjustments to the parameters of more than one mode. In this sense, it is useful to identify the rates at which each mode contributes. This can be achieved by comparing $\dot{\epsilon}$ against the reciprocal stretch relaxation times $1/\tau_{s_0 i}$. With respect to the effects of the different parameters on the response of a single mode we note the following:

(1) As in the original pom-pom model, at rates $\dot{\epsilon} \gtrsim 1/\tau_{s_0}$, the most efficient way to control extensional hardening, during startup of the flow, is by adjusting the parameters τ_{d_0}/τ_{s_0} and q. Increases in the former parameter lead to weaker hardening, whereas increases in the latter parameter lead to higher hardening.

(2) As regards the overshoots, at rates at which the maximum stretch is achieved, their magnitude at both shear and extension is readily controlled by Ψ_w; by decreasing Ψ_w one gets larger overshoots and thus lower viscosity steady states. In such occasions, and for given values of τ_{d_0}/τ_{s_0} and Ψ_w, variations in h over a reasonable range, i.e., 1–2 U, do not typically influence the magnitude of the overshoot unless Ψ_w is low (that is, $0.1 \lesssim \Psi_w \lesssim 0.3$). At rates at which no maximum stretch is achieved the overshoot can be controlled by both Ψ_w and h: Decreases in Ψ_w act in the same direction as increases in h, i.e., such variations lead to larger overshoots.

(3) As Ψ_w approaches unity the predictions tend to the original pom-pom model. In other words, overshoots weaken as Ψ_w increases. With respect to extension, they vanish when $\Psi_w = 1$.

(4) As regards the stress relaxation behavior (RC), we notice that increases (decreases) in h (Ψ_w) lead to much faster relaxation in the **AO** case than in the **BO** case. Such changes in the parameters, from the perspective of achieving much more rapid relaxation in the **AO** case than in the **BO** case, are meaningful for the slowest modes. For fast modes, though stress relaxes quicker in the **AO** case, the **AO** and **BO** curves do never cross each other during the early and intermediate stages of the relaxation phase.

V. MULTIMODE MODEL

A. Full model

We now attempt to fit the FSR data of the DOW 150 R sample using a multimode version of the overshoot model developed in Sec. III C. In the remainder of this paper, this version of the model will be referred to as the full model. Figure 7 compares the predictions of the full model (lines) with the experimental data (symbols). The upper, left panel also shows shear data [Hassell *et al.* (2008)] together with model predictions. The theoretical curves are obtained using the parameterization shown in Table II. This parameterization is comprised of only three stretching modes with $q \neq 1$. In Fig. 7, as in Fig. 8, we do not represent the extensional rates in Weissenberg numbers because the LDPE sample has a broad spectrum of stretch relaxation times.

With respect to shear, the full model provides a good fit to the data apart the lowest rates for which the overshoot is overestimated. Concerning the extensional flow, it also shows a good agreement with the FSR data at the three highest strain rates. However, it (i) seriously underestimates the hardening at the lowest nonlinear strain rate (r2). (ii) Foremost, it fails to capture the different stress relaxation behavior before and after the overshoot at $\dot{\epsilon} = 0.1\text{s}^{-1}$; with this parameterization, no strong crossing of the theoretical **AO** and **BO** relaxation curves occurs at this particular strain rate.

By altering parameterization, it is possible to improve the predictions of the full model with respect to shortcomings (i) or (ii) above. Nevertheless, it is impossible to overcome

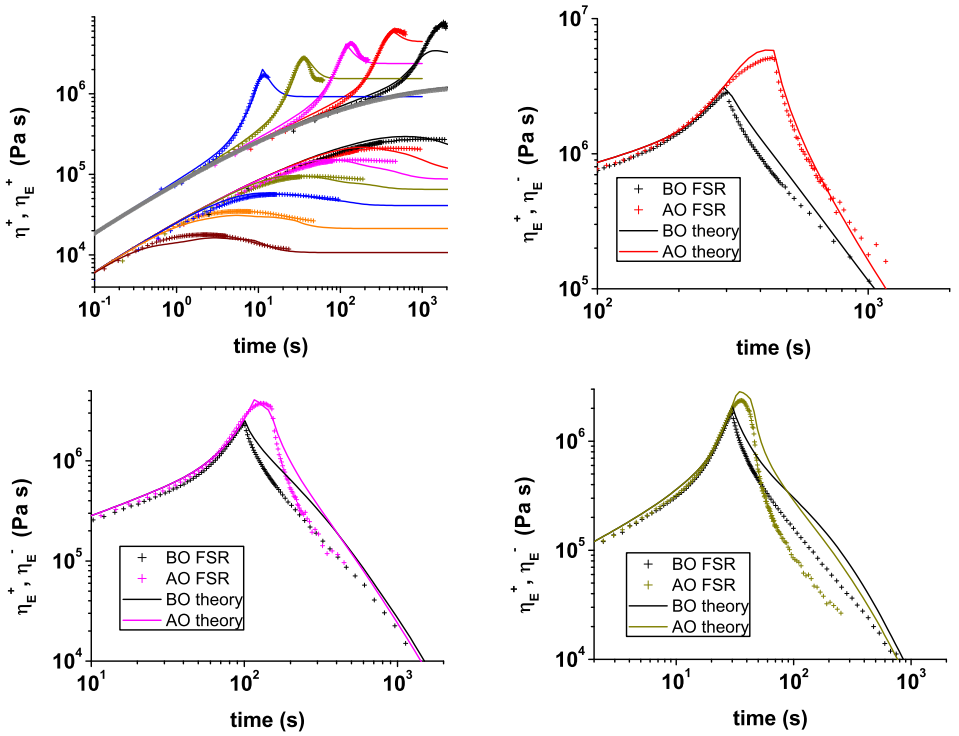

FIG. 7. Comparison of the full model (lines) with the FSR data (symbols) for extension, and shear data [Hassell *et al.* (2008)], for the DOW 150 R sample. The theoretical lines have been obtained using the parameterization shown in Table II. NC for shear and extension (upper, left). RC following the extensional flow: $\dot{\epsilon} = 0.01\text{s}^{-1}$ (upper right), $\dot{\epsilon} = 0.03\text{s}^{-1}$ (bottom left), and $\dot{\epsilon} = 0.1\text{s}^{-1}$ (bottom right). For each rate, the flow has been stopped at $\epsilon_0 = 3$ and $\epsilon_0 = 4.5$ for the **BO** and **AO** case, respectively. Color code for the rates is explained in Table IV.

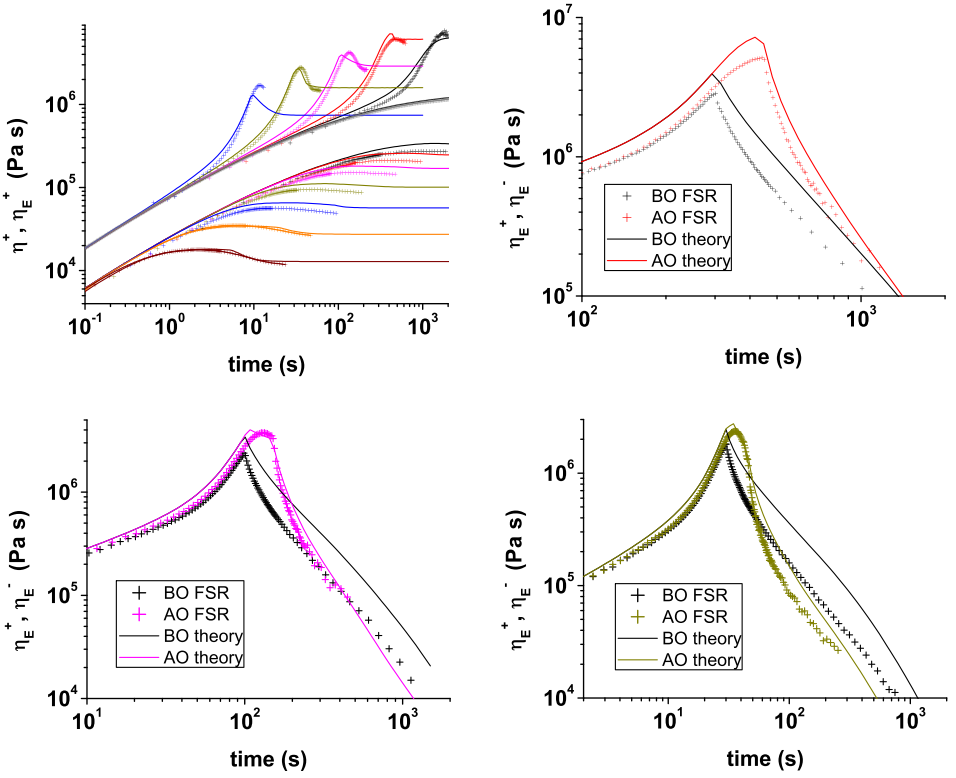

FIG. 8. Comparison of the minimal model (lines) with the FSR data (symbols) for extension and shear data [Hassell *et al.* (2008)], for the DOW 150 R sample, using the parameterization shown in Table III. NC for shear and extension (upper, left). RC following the extensional flow: $\dot{\epsilon} = 0.01\,\mathrm{s}^{-1}$ (upper right), $\dot{\epsilon} = 0.03\,\mathrm{s}^{-1}$ (bottom left), and $\dot{\epsilon} = 0.1\,\mathrm{s}^{-1}$ (bottom right). For each rate, the flow has been stopped at $\epsilon_0 = 3$ and $\epsilon_0 = 4.5$ for the **BO** and **AO** case, respectively. The color code for the rates is the same as in Fig. 7 and is explained in Table IV.

both shortcomings using a single parameterization; when the slowest modes are decorated with values of Ψ_w and h that enhance stress relaxation following the overshoot, then the model seriously underestimates the hardening (stretch) at the lowest strain rates (for the NC in extension). In conclusion, with respect to the extensional flow, the full model can either fit the data of the NC or the data of the RC, but it cannot simultaneously fit both sets of data with a single parameterization. In what follows, we will present a minimal model that largely overcomes this shortcoming of the full model.

B. Minimal model

Here, we neglect ES before the maximum stretch condition thus the only process that contributes to ES is branch point withdrawal. That is, in the minimal model the retraction rate is given by

$$w = \begin{cases} 0 & \text{for } \lambda < q \\ -\mathbf{K} : \mathbf{S} & \text{for } \lambda \geq q. \end{cases} \tag{17}$$

Our rationale for making this assumption is mainly for the purposes of simple and uncomplicated fitting of data: We retain the simplicity of the pom-pom model (no ES) before branch-

point withdrawal, but include ES beyond branch-point withdrawal to give the overshoots. We suspect that the full model includes some but not all of the true physics and so (unfortunately) performs worse in data fitting. The minimal model has the advantage that the slowest modes, which do not typically achieve maximum stretch at the lowest strain rates, exhibit significantly higher hardening than in the full model. Figure 8 compares the predictions of the minimal model with the FSR measurements. (Color code and symbols are exactly the same as in Fig. 7.) It has been obtained using the parameterization presented in Table III.

According to the upper panel of Fig. 8, the minimal model compares much better with the data than the full model at the lowest extensional rate. Here, the extensional (steady state) viscosity is within the experimental error (see upper panel of Fig. 1). This is also the case at rates r4 and r5; nevertheless, for those rates, the cross-slot flow measurements [Hoyle (2011); Auhl *et al.* (2011)] indicate that the steady state is even lower than the apparent steady state of the FSR data. At the highest rate, the maximum is slightly underestimated. At this rate, a steady state is not achieved in the FSR. The minimal model overestimates by 20% the steady state measurement of the cross-slot experiment [Hoyle (2011); Auhl *et al.* (2011)]. The model also provides a reasonable fit to the shear data.

As regards the RC, shown at the upper right and bottom panels of Fig. 8, the predictions of the minimal model are in qualitative agreement with the data. For all examined rates, the model correctly forecasts that the relaxation is faster in the **AO** case than in the **BO** case. Moreover, for the r5 rate, the predicted crossing of the **AO** and **BO** relaxation curves is similar to the one seen in the measurements. However, the model predictions are not in full quantitative agreement with the data, especially for the case at which the flow is stopped before the overshoot since ES has been neglected before the maximum stretch. Overall, the minimal version of the overshoot model provides a reasonable, but not perfect, fit to all experimental data with a single parameterization set.

It should be stressed, however, that the superior performance of the minimal model in fitting the experimental data does not necessarily render the minimal model superior to the full model from the physical point of view. The physical reason, if any, behind the superior performance of the minimal model is not obvious. It may be that there is actually a fundamental difference between (i) the stretch relaxation process (via branch point hopping), which involves contour length fluctuations at the same time as stretch relaxation, and (ii) branch-point withdrawal, which is a sudden process involving, in some sense, a change of state of the molecules. While this is speculative, it does point toward the form of the minimal model.

An alternative (and perhaps more likely) possibility is that the coupling of different pom-pom modes gives rise to additional effects not captured in the current decoupled approximation. It is, unfortunately, often the case that decoupled and simplified multimode models demonstrate superior performance over detailed models, but sometimes at the expense of representing the physics fully. For example, for linear polymers (which is a much simpler situation than the present case), the detailed "GLaMM" model of Graham *et al.* (2003) requires nonzero CCR in order to fit data. In contrast, the simplified multimode "Rolie-Poly" model [Graham and Likhtman (2003)] fits data best with the CCR parameter set to zero. Again the issue is the lack of coupling between modes in the multimode approximation.

VI. CONCLUSIONS

The primary purpose of this work was to investigate, at the semiphenomenological level of the pom-pom model, a candidate explanation for two surprising features recently observed in FSR experiments of uniaxial extensional flow of industrial branched polymer resins: (i) Overshoots of the transient stress during steady flow, and (ii) strongly accelerated stress relaxation upon cessation of the flow beyond the overshoot. We proposed that a

candidate explanation for these two effects is "ES"—a loss of entanglements due to relative motion of polymer chains caused by flow and chain retraction. We noted that, in the context of branched polymers, the "branch-point withdrawal" process provides occasion for a sudden increase in the degree of ES and that loss of entanglements is likely to lead to an exponential increase in relaxation rates. We demonstrated that inclusion of these two effects could indeed qualitatively reproduce the experimental observations in a single mode version of the model. We have additionally shown that the incorporation of ES in the mPP formalism can provide a practical tool for fitting transient viscosity data of industrial melts that exhibit overshoots under steady, uniaxial extensional flow. We consider that our successful comparison with experimental data is indicative that ES is a viable hypothesis to explain the stress overshoots and anomalous stress relaxation. However, the mPP approach necessarily involves a large number of fitting parameters; thus, confirmation of this proposed mechanism requires a more detailed molecular-level investigation.

We argued that the physical origin of the extensional overshoot is the strong ES that follows the branch point withdrawal process, which, in turn, is triggered by sufficiently high strains and strain rates. Hence, we anticipate molecules with higher degree of branching to exhibit larger overshoots than less branched molecules since the value of the strain, and chain stretch, is larger at the onset of branch-point withdrawal, giving rise to a more sudden onset of ES. For the DOW 150 R sample considered in the present work, the maximum stretch of the stress-carrying chains (leading to branchpoint withdrawal) occurs at strains between 3 and 4.5, so this is the range of strain within which the strong stress overshoots are observed for this sample. This argument can qualitatively explain why heavily branched structures like LDPEs, as well as highly branched metallocenes like the HDB6 sample [Hoyle *et al*. (2013)], have higher tendency for extensional overshoots than model branched structures like pom-pom-like [Nielsen *et al*. (2006)] and H-shaped polystyrene molecules [Huang (2013)]. In contrast to branching, polydispersity does not appear to be a key factor for the appearance of overshoots: For a commercial PS melt (of linear chains) with high polydispersity (PDI = 3.7), no stress overshoot has been observed over a wide range of strain rates [Huang (2013)].

The difficulty in fitting all data simultaneously may be an indication that different modes (sections of the LCB molecule) are coupled in their dynamics, a fact which is fully ignored in the present multimode approximation. An additional piece of physics not included in the present model (nor in the original pom-pom model) is the nested tube structure and different types of stress relaxation suggested by constraint release within the dynamic dilution approximation. In the linear rheological limit, stress is relaxed both by tube escape and by constraint release [Das *et al*. (2014)]. It seems probable that, in nonlinear flow, such effects would couple with the ES identified within the present work. This is simply a further indication that reality is likely to be significantly more complicated than the very simplified model developed here.

During the course of this work, we identified an anomaly in the differential version of the original pom-pom model with regard to relaxation after steady extensional flow: The effective relaxation time of the orientation is massively increased, in a wholly unphysical manner. We discussed the reasons for this and suggested a suitable alternative.

Several possible extensions to the present work suggest themselves. As noted in the introduction hints of ES are observed in molecular dynamics simulations of linear polymers [Sefiddashti *et al*. (2015)] and in slip-link simulations [Masubuchi *et al*. (2012, 2014); Andreev *et al*. (2013)]: These methods may provide corroboration of the assumptions in the present model for branched polymers. A more detailed tube model description of branched polymer dynamics might seek to capture the nested tube structure suggested by constraint release models, and to couple the dynamics of adjacent polymer

segments in a branched molecule. Also, the model is not detailed enough to capture the effect of entangled/unentangled branches on the overshoot and stress relaxation (entangled branches are considered here). Finally, various deformation histories may be investigated, such as strain recovery [Nielsen and Rasmussen (2008)] or other reversing flow situations, which are evidently related to the present stress recovery experiments. In the specific context of reversing flow, we note that modifications to the pom-pom model have previously been proposed [Lee *et al.* (2001)]. Considerations such as these would be needed also if the present model were applied in reversing flow.

ACKNOWLEDGMENTS

This work was financially supported by the European Union through the "Dynacop" Marie Curie 7th Framework Initial Training network. The authors would also like to thank Dr. David M. Hoyle from the University of Durham for helpful discussions.

APPENDIX A: POM-POM SPECTRA

This Appendix provides the pom-pom spectra used in the comparison of our multimode model with the experimental data. Specifically, Tables II and III present the parameterization for the full and minimal model, respectively.

According to Tables II and III, the eight modes overshoot model requires 48 parameters to function. This is not entirely the case despite the fact that each mode consists of six parameters. In fact, regardless of their exact number, about two thirds of the modes are inactive in terms of the nonlinear parameter, q. That is, for these modes $q = \lambda = 1$. Since the stretch is at its equilibrium value, the retraction process and, in turn, the ES process is inactive in the model. This practically means that τ_{d0}/τ_{s0} and Ψ_w can be set to unity, while h can be set to zero. Hence, between the nonstretching modes, only the linear parameters, G_0 and τ_{d0}, differ. This fact significantly reduces the total number of parameters of the multimode model.

It is obvious that the number of fitting parameters can be further reduced by using fewer modes: Two to three modes per decade are typically required to capture the linear viscoelastic response, i.e., small amplitude oscillatory (SAOS) data, of an industrial sample. This practical rule indicates that ten to fifteen modes are required for the DOW 150R sample since its oscillatory frequency data cover five decades; nevertheless, to minimize the number of fitting parameters in our model, we have used the minimum number of modes (eight) that is required to reasonably fit the SAOS data.

TABLE II. Parameterization for the full version of the model.

DOW 150 R at 160 °C, 15 modes						
Mode	G_{0_i} (Pa)	$\tau_{d0\,i}$ (s)	$\frac{\tau_{d0\,i}}{\tau_{s0\,i}}$	q	Ψ_w	H
1	1.1×10^5	3.5×10^{-3}	1.0	1	1.0	0.0
2	4.3×10^4	2.1×10^{-2}	1.0	1	1.0	0.0
3	3.0×10^4	1.2×10^{-1}	1.0	1	1.0	0.0
4	1.6×10^4	7.1×10^{-1}	1.0	1	1.0	0.0
5	8.1×10^3	4.2	1.0	1	1.0	0.0
6	3.3×10^3	24.5	3.00	7	0.50	1.20
7	949	144.3	2.00	13	0.30	1.00
8	157	848	1.10	15	0.45	0.70

TABLE III. Parameterization for the minimal model.

DOW 150 R at 160 °C, 15 modes						
Mode	G_{0_i} (Pa)	$\tau_{d_0 i}$ (s)	$\frac{\tau_{d_0 i}}{\tau_{s_0 i}}$	q	Ψ_w	H
1	1.1×10^5	3.5×10^{-3}	1.0	1	1.0	0.0
2	4.3×10^4	2.1×10^{-2}	1.0	1	1.0	0.0
3	3.0×10^4	1.2×10^{-1}	1.0	1	1.0	0.0
4	1.6×10^4	7.1×10^{-1}	1.0	1	1.0	0.0
5	8.1×10^3	4.2	6.0	5	1.0	0.0
6	3.3×10^3	24.5	3.0	6	0.1	1.0
7	949	144.3	1.8	8	0.1	0.45
8	157	848	1.15	11	0.1	0.40

Finally, we note that the size of the overshoot model parameter space is restricted by the following physical constraints: τ_{d_0}/τ_{s_0} and h must decrease, whereas q must increase, toward the center of a LCB molecule. These constraints arise from the hierarchical character of the relaxation of a LCB molecule.

APPENDIX B: ABBREVIATIONS

TABLE IV. Abbreviations.

NC	The *normal case*, i.e., the flow condition in which the melt is subjected to steady uniaxial extensional flow
RC	The *relaxation case*, i.e., the case that involves cessation of the extensional flow. Here, $\dot{\epsilon} = 0.1\,\mathrm{s}^{-1}$
AO	The flow is ceased after the overshoot
BO	The flow is ceased before the overshoot
ES	Entanglement stripping
r1	$\dot{\epsilon} = 0.0001\,\mathrm{s}^{-1}$. Gray color in Figs. 7 and 8
r2	$\dot{\epsilon} = 0.003\,\mathrm{s}^{-1}$. Black color in Figs. 7 and 8
r3	$\dot{\epsilon} = 0.01\,\mathrm{s}^{-1}$. Red color in Figs. 7 and 8
r4	$\dot{\epsilon} = 0.03\,\mathrm{s}^{-1}$. Magenta color in Figs. 7 and 8
r5	$\dot{\epsilon} = 0.1\,\mathrm{s}^{-1}$. Dark yellow color in Figs. 7 and 8
r6	$\dot{\epsilon} = 0.3\,\mathrm{s}^{-1}$. Blue color in Figs. 7 and 8
r7	$\dot{\epsilon} = 1\,\mathrm{s}^{-1}$. Orange color in Figs. 7 and 8
r8	$\dot{\epsilon} = 3\,\mathrm{s}^{-1}$. Wine color in Figs. 7 and 8
$\eta_E^+(t, \dot{\epsilon})$	Tensile stress growth coefficient (or transient viscosity)
$\eta_E^-(t, \dot{\epsilon})$	Tensile stress decay coefficient
$\eta_E(\dot{\epsilon})$	Extensional viscosity, i.e., $\eta_E^+(t \to \infty, \dot{\epsilon})$

References

Andreev, M., R. N. Khaliullin, R. J. A. Steenbakkers, and J. D. Schieber, "Approximations of the discrete slip-link model and their effect on nonlinear rheology predictions," J. Rheol. **57**, 535–557 (2013).

Auhl, D., D. M. Hoyle, D. Hassell, T. D. Lord, O. G. Harlen, M. R. Mackley, and T. C. B. McLeish, "Cross-slot extensional rheometry and the steady-state extensional response of long chain branched polymer melts," J. Rheol. **55**, 875–900 (2011).

Auhl, D., P. Chambon, T. C. B. McLeish, and D. J. Read, "Elongational flow of blends of long and short polymers: Effective stretch relaxation time," Phys. Rev. Lett. **103**, 136001 (2009).

Bach, A., H. K. Rasmussen, and O. Hassager, "Extensional viscosity for polymer melts measured in the filament stretching rheometer," J. Rheol. **47**, 429–441 (2003).

Blackwell, R. J., T. C. B. McLeish, and O. G. Harlen, "Molecular drag-strain coupling in branched polymer melts," J. Rheol. **44**, 121–136 (2000).

Burghelea, T. I., Z. Starý, and H. Münstedt, "On the viscosity overshoot during the uniaxial extension of a low density polyethylene," J. Non-Newtonian Fluid Mech. **166**, 1198–1209 (2011).

Clemeur, N., R. P. G. Rutgers, and B. Debbaut, "On the evaluation of some differential formulations for the Pompom constitutive model," Rheol. Acta **42**, 217–231 (2003).

Clemeur, N., R. P. G. Rutgers, and B. Debbaut, "Numerical simulation of abrupt contraction flows using the double convected Pompom model," J. Non-Newtonian Fluid Mech. **117**, 193–209 (2004).

Das, C., D. J. Read, D. Auhl, M. Kapnistos, J. den Doelder, I. Vittorias, and T. C. B. McLeish, "Numerical prediction of nonlinear rheology of branched polymer melts," J. Rheol. **58**, 737–757 (2014).

Graham, R. S., and A. E. Likhtman, "Simple constitutive equation for linear polymer melts derived from molecular theory: RoliePoly equation," J. Non-Newtonian Fluid Mech. **114**, 1–12 (2003).

Graham, R. S., A. E. Likhtman, T. C. B. McLeish, and S. T. Milner, "Microscopic theory of linear, entangled polymer chains under rapid deformation including chain stretch and convective constraint release," J. Rheol. **47**, 1171–1200 (2003).

Hassell, D., D. Auhl, T. C. B. McLeish, O. G. Harlen, and M. R. Mackley, "The effect of viscoelasticity on stress fields within polyethylene melt flow for a cross-slot and contraction-expansion slit geometry," Rheol. Acta **47**, 821–834 (2008).

Hoyle, D. M., "Constitutive modelling of branched polymer melts in non-linear response," Ph.D. thesis, University of Leeds, Leeds, United Kingdom, 2011.

Hoyle, D. M., Q. Huang, D. Auhl, D. Hassell, H. K. Rasmussen, A. L. Skov, O. G. Harlen, O. Hassager, and T. C. B. McLeish, "Transient overshoot extensional rheology of long-chain branched polyethylenes: Experimental and numerical comparisons between filament stretching and cross-slot flow," J. Rheol. **57**, 293–313 (2013).

Huang, Q., "Molecular rheology of complex fluids," Ph.D. thesis, Technical University of Denmark, Lyngby, Denmark, 2013.

Huang, Q., H. K. Rasmussen, A. L. Skov, and O. Hassager, "Stress relaxation and reversed flow of low-density polyethylene melts following uniaxial extension," J. Rheol. **56**, 1535–1554 (2012).

Ianniruberto, G., "Quantitative appraisal of a new CCR model for entangled linear polymers," J. Rheol. **59**, 211–235 (2015).

Ianniruberto, G., and G. Marrucci, "Convective constraint release (CCR) revisited," J. Rheol. **58**, 89–102 (2014).

Inkson, N. J., T. C. B. McLeish, O. G. Harlen, and D. J. Groves, "Predicting low density polyethylene melt rheology in elongational and shear flows with 'pom-pom' constitutive equations," J. Rheol. **43**, 873–896 (1999).

Lee, K., M. R. Mackley, T. C. B. McLeish, T. M. Nicholson, and O. G. Harlen, "Experimental observation and numerical simulation of transient 'stress fangs' within flowing molten polyethylene," J. Rheol. **45**, 1261–1277 (2001).

Lentzakis, H., D. Vlassopoulos, D. J. Read, H. Lee, T. Chang, P. Driva, and N. Hadjichristidis, "Uniaxial extensional rheology of well-characterized comb polymers," J. Rheol. **57**, 605–625 (2013).

Marín, J. M. R., J. K. Huusom, N. J. Alvarez, Q. Huang, H. K. Rasmussen, A. Bach, A. L. Skov, and O. Hassager, "A control scheme for filament stretching rheometers with application to polymer melts," J. Non-Newtonian Fluid Mech. **194**, 14–22 (2013).

Masubuchi, Y., Y. Matsumiya, H. Watanabe, G. Marrucci, and G. Ianniruberto, "Primitive chain network simulations for pom-pom polymers in uniaxial elongational flows," Macromolecules **47**, 3511–3519 (2014).

Masubuchi, Y., Y. Matsumiya, H. Watanabe, S. Shiromoto, M. Tsutsubuchi, and Y. Togawa, "Primitive chain network simulations for comb-branched polymer under step shear deformations," Rheol. Acta **51**, 193–200 (2012).

McKinley, G. H., and T. Sridhar, "Filament-stretching rheometry of complex fluids," Annu. Rev. Fluid Mech. **34**, 375–415 (2002).

McLeish, T. C. B., "Tube theory of entangled polymer dynamics," Adv. Phys. **51**, 1379–1527 (2002).

McLeish, T. C. B., and R. G. Larson, "Molecular constitutive equations for a class of branched polymers: The pom-pom polymer," J. Rheol. **42**, 81–110 (1998).

Meissner, J., and J. Hostettler, "A new elongational rheometer for polymer melts and other highly viscoelastic liquids," Rheol. Acta **33**, 1–21 (1994).

Münstedt, H., and D. Auhl, "Rheological measuring techniques and their relevance for the molecular characterization of polymers," J. Non-Newtonian Fluid Mech. **128**, 62–69 (2005).

Nielsen, J. K., and H. K. Rasmussen, "Reversed extension flow," J. Non-Newtonian Fluid Mech. **155**, 15–19 (2008).

Nielsen, J. K., H. K. Rasmussen, M. Denberg, K. Almdal, and O. Hassager, "Nonlinear branch-point dynamics of multiarm polystyrene," Macromolecules **39**, 8844–8853 (2006).

Nielsen, J. K., H. K. Rasmussen, and O. Hassager, "Stress relaxation of narrow molar mass distribution polystyrene following uniaxial extension," J. Rheol. **52**, 885–899 (2008).

Rasmussen, H. K., A. G. Bejenariu, O. Hassager, and D. Auhl, "Experimental evaluation of the pure configurational stress assumption in the flow dynamics of entangled polymer melts," J. Rheol. **54**, 1325–1336 (2010).

Rasmussen, H. K., J. K. Nielsen, A. Bach, and O. Hassager, "Viscosity overshoot in the start-up of uniaxial elongation of low density polyethylene melts," J. Rheol. **49**, 369–381 (2005).

Read, D. J., K. Jagannathan, S. K. Sukumaran, and D. Auhl, "A full-chain constitutive model for bidisperse blends of linear polymers," J. Rheol. **56**, 823–873 (2012).

Sefiddashti, M. H. N., B. J. Edwards, and B. Khomami, "Individual chain dynamics of a polyethylene melt undergoing steady shear flow," J. Rheol. **59**, 119–153 (2015).

Sentmanat, M., B. N. Wang, and G. H. McKinley, "Measuring the transient extensional rheology of polyethylene melts using the SER universal testing platform," J. Rheol. **49**, 585–606 (2005).

Verbeeten, W. M. H., G. W. M. Peters, and F. P. T. Baaijens, "Differential constitutive equations for polymer melts: The extended Pompom model," J. Rheol. **45**, 823–843 (2001).

Wagner, M. H., and V. H. Rolón-Garrido, "Verification of branch point withdrawal in elongational flow of pom-pom polystyrene melt," J. Rheol. **52**, 1049–1068 (2008).

Wang, Y., S. Cheng, and S. Q. Wang, "Basic characteristics of uniaxial extension rheology: Comparing monodisperse and bidisperse polymer melts," J. Rheol. **55**, 1247–1270 (2011).